DOI 10.1002/2017GC006948

Generation of silicic melts in the early Izu-Bonin arc recorded by detrital zircons in proximal arc volcaniclastic rocks from the Philippine Sea

Barth, A.P.[1], Tani, K.[2], Meffre, S.[3], Wooden, J.L.[4], Coble, M.A.[5], Arculus, R.J.[6], Ishizuka, O.[7], Shukle, J.T.[1]

[1]Department of Earth Sciences, Indiana University~Purdue University Indianapolis, Indianapolis, IN 46202

[2]Department of Geology and Paleontology, National Museum of Nature and Science, Tsukuba, Japan

[3]CODES ARC Centre of Excellence in Ore Deposits, University of Tasmania

[4]U.S. Geological Survey, Menlo Park, CA (retired)

[5]Department of Geological Sciences, Stanford University, Stanford, CA

[6]Research School of Earth Sciences, Australian National University, Acton, Australia

[7]Geological Survey of Japan/AIST, Tsukuba, Japan

Key Points:

- Detrital zircons preserve age and trace element evidence of oceanic arc provenance
- Zircons record 16 million years of early arc silicic melt evolution
- Silicic melts indicate arc asymmetry developed about 10 Ma following arc initiation

Abstract

A 1.2 kilometer thick Paleogene volcaniclastic section at International Ocean Discovery Program Site 351-U1438 preserves the deep-marine, proximal record of Izu-Bonin oceanic arc initiation and volcano evolution along the Kyushu-Palau Ridge (KPR). Pb/U ages and trace element compositions of zircons recovered from volcaniclastic sandstones preserve a remarkable temporal record of juvenile island arc evolution. Pb/U ages ranging from 43 to 27 Ma are compatible with provenance in one or more active arc edifices of the northern KPR. The abundances of selected trace elements with high concentrations provide insight into the genesis of U1438 detrital zircon host melts, and represent useful indicators of both short and long-term variations in melt compositions in arc settings. The Site U1438 zircons span the compositional range between zircons from mid-ocean ridge gabbros and zircons from relatively enriched continental arcs, as predicted for melts in a primitive oceanic arc setting derived from a highly depleted mantle source. Melt zircon saturation temperatures and Ti-in-zircon thermometry suggest a provenance in relatively cool and silicic melts that evolved toward more Th and U-rich compositions with time. Th, U and light rare earth element enrichments beginning about 35 Ma are consistent with detrital zircons recording development of regional arc asymmetry and selective trace element-enriched rear arc silicic melts as the juvenile Izu-Bonin arc evolved.

Index Terms: 1065, 1165, 8185

1. Introduction

Understanding the petrologic evolution of oceanic arc magmas through time is important because these arcs reveal the processes of formation and early evolution of juvenile continental crust. The

compositions of oceanic arc lavas broadly mimics average granodioritic (andesitic) continental crust (e.g. Taylor, 1967), yet the common basaltic-andesitic lavas in these settings are typically relatively depleted in lithophile minor and trace elements compared to average continental crust (Rudnick and Gao, 2004). However, a key characteristic of many oceanic arcs is the observed increase, inboard from the volcanic front, of incompatible and especially lithophile element abundances (e.g. Gill, 1981). For example, low K basalts and andesites along the Izu-Bonin volcanic front in the western Pacific have significantly lower U, Th, Th/U and are depleted in rare earth elements (REE) compared to medium- and high-K rear arc lavas, the latter being comparable to average granodioritic continental crust (e.g., Hochstaedter et al., 2001; Ishizuka et al., 2003, 2006a; Tamura et al., 2010; Kimura et al., 2010; Tani et al., 2015). Therefore, for a full accounting of the genesis of juvenile continental crust we need to understand spatial and temporal variations within such geochemically asymmetrical oceanic arcs that lead to generation of these more enriched silicic magmas in oceanic arc settings.

In this report we describe the utility of zircons from proximal arc-derived volcaniclastic rocks for constraining the temporal evolution of silicic rear arc magmas in a prototypical oceanic arc, the Izu-Bonin-Mariana (IBM) arc system of the western Pacific. Arc-derived forearc and back-arc volcaniclastic sequences provide important long-term records of magmatic evolution that complement bedrock sampling of incompletely exposed arc edifices and dredging of submerged arc surfaces (Dickinson, 1974, 1982; Gill et al., 1994, Arculus et al., 1995; Draut and Clift, 2006, 2013). Detrital zircon can augment petrographic and bulk geochemical studies of these arc volcaniclastic rocks because, through analyses of Pb/U and trace elements, zircons provide

closely-coupled temporal and geochemical records of silicic melt evolution (Walker et al., 2010; Barth et al., 2013; Kern et al., 2016).

We describe detrital zircons recovered from proximal volcaniclastic rocks deposited on the distal (relative to the trench) flank of the early IBM arc, with the goal of quantifying the timing and geochemical nature of rear arc silicic melt formation following intraoceanic arc initiation. Pb/U ages of detrital zircons recovered at International Ocean Discovery Program (IODP) Site 351-U1438 provide precise maximum depositional ages that reinforce shipboard biostratigraphy and magnetostratigraphy of the volcaniclastic sequence. Trace element abundances and ratios of these zircons are compared to regional and global zircon suites. These new data indicate that detrital zircons yield insights into the generation of silicic melts early in the evolutionary history of the Izu-Bonin oceanic arc. Furthermore, the internally-consistent data sets of oceanic arc-derived zircon generated by this project will form a set of useful geochemical proxies for interpreting detrital zircon provenance.

2. Geologic Setting

The IBM arc system (**Figure 1**) has been targeted for studies of oceanic arc evolution because it is one of several western Pacific intraoceanic arcs initiated ~50 Ma (Stern, 2004; Arculus et al., 2015a) and because of its prominent spatial asymmetry with widespread development of relatively enriched rear arc lavas (Hochstaedter et al., 2000, 2001; Tamura et al., 2009, 2013; Tollstrup et al., 2010). Understanding the IBM system has broad significance for global studies of subduction initiation, arc inception and subsequent arc evolution. The IBM system shows

clear evidence for intraoceanic arc inception in early Eocene time (Ishizuka et al., 2011a), and geomorphic and geochronologic evidence indicates early oceanic arc evolution is preserved in a remnant arc, the Kyushu-Palau Ridge (KPR). The KPR forms the western margin of the Shikoku and Parece Vela basins, the locus of Miocene rifting that separated the KPR from the modern, active Izu-Bonin arc (Ishizuka et al., 2011b). Geochemical evidence from volcaniclastic rocks and tephra glasses suggests both spatial and temporal variation in melt chemistry as the arc evolved (Gill et al., 1994; Straub, 2003, Straub et al., 2015), and geophysical evidence from velocity models indicates arc evolution was associated with formation of a broadly 'continental' (i.e., tonalitic) middle crust in this intraoceanic setting (Nishizawa et al., 2007; Kodaira et al., 2007; Takahashi et al., 2007, 2008, 2009).

For these reasons, IODP Project IBM identified three drilling targets in the forearc, back-arc and west of the KPR remnant arc to elucidate the nature of pre-existing arc crust, the subduction initiation process, and spatial–temporal variations in arc magmatism. Recovering a sedimentary record of early IBM magmatism following arc initiation was one of the key objectives of Expedition 351 in the proximal rear arc of the IBM system. $^{40}Ar/^{39}Ar$ ages of cored and dredged samples suggest volcanism in the KPR was active until 28 to 25 Ma (Ishizuka et al., 2011b; Fig. 3), and the enriched compositions of many KPR lavas suggest a rear arc affinity. A temporally well-constrained record of initiation and evolution of Paleogene magmatism in the KPR is important because these magmas more closely approximate juvenile continent crust, and their distinctive rare earth and high field strength element abundances should be recognizable in high frequency sampling of the volcaniclastic record.

IODP Expedition 351 drilling at Site U1438 recovered a basement and sedimentary record of arc initiation from the Amami Sankaku Basin, the proximal back-arc of the northern KPR (**Figures 1 and 2**; Arculus et al., 2015a). The principal drilling objectives for this site were to characterize the nature of the igneous crust and mantle prior to IBM arc inception and to characterize the Paleogene compositional evolution of the nascent IBM magmatic arc utilizing the volcaniclastic record overlying basement. Four stratigraphic units above basement were cored at Site 351-U1438 (Arculus et al., 2015b; hereafter 'U1438' for brevity). Unit I is comprised of Oligocene to recent terrigenous and biogenic mud with discrete tephra layers. Units II, III and IV are Eocene to Oligocene volcaniclastic rocks, increasingly lithified and hydrothermally altered with depth, which constitute a ~1.2 km thick sedimentary record of KPR arc initiation and evolution. The overall pattern of upward coarsening through Unit III is interpreted to record building of the early arc edifices. Abrupt fining of the upper ~200 m of the section in Unit II is interpreted to record the waning and demise of the arc with onset of rifting of the active arc away from the KPR by opening of the Shikoku Basin.

A section comparable to U1438 was recovered on Ocean Drilling Program (ODP) Leg 195 at Site 1201 in the proximal back-arc of the southern KPR (**Figure 1**; Salisbury et al., 2006). Although the section at Site 1201 is thinner than at U1438, aspects of the sedimentary sequences are strikingly similar (**Figure 2**). A thin Eocene pelagic section is overlain by late Eocene through Oligocene volcaniclastic turbidites derived from the KPR, followed by a transition to late Oligocene and Neogene deep-sea pelagic sedimentation after extinction of the KPR arc.

3. Sampling

3.1. IODP Sites 351-U1438 and 195-1201

Drill core samples of medium to coarse-grained, massive to laminated sandstones from Units II, III, and IV at U1438 and Unit II at Site 1201 were collected as 7 to 10 cm quarter-rounds from working core halves and as half- and whole-rounds from core catcher material. Samples were rinsed and ultrasonicated in deionized water, cleaned by grinding all cut surfaces with SiC paper, ultrasonicated twice more, and air dried. The cleaned core samples were disaggregated with a high-voltage electric pulse fragmentation device (SELFRAG Lab) and zircons were concentrated using conventional panning and purification using methylene iodide.

3.2. IODP Expedition 351 Drilling Mud

Drill core samples may be contaminated by mud added to drilling fluids to sweep and stabilize a borehole during hard-rock drilling with a rotary core barrel system. JOIDES Resolution used a sepiolite drilling mud on Expedition 351 that contained detrital zircons. In order to provide a quantitative framework for evaluating possible contamination of U1438 drill cores, zircons were recovered from a shipboard sample of this drilling mud using standard gravimetric techniques.

3.3. Dredge Samples

Intrusive igneous rocks dredged from the KPR and Parece Vela Basin provide monogenetic zircon suites for comparison with polygenetic populations of detrital zircons. Sample D08B-02 is

a 37.5 Ma biotite hornblende tonalite dredge sample from the south side of Komahashi-Daini Seamount on the northern KPR, and was described by Haraguchi et al. (2003). Sample MKH is a 48.5 Ma granodiorite dredge sample from Minami-Koho Seamount on the northern KPR, and was described by Ishizuka et al. (2011b). We compare these KPR samples to broadly coeval dredge samples of early Eocene intrusive igneous rocks from Santa Rosa Bank in the forearc of the southern IBM (Reagan et al., 2013). Between the KPR and the Marianas, samples D7-002 and D18-002 are 11 to 12 Ma oxide gabbro and plagiogranite, respectively, dredged from the Godzilla oceanic core complex, which lies along the southwestern side of the spreading center in the southern Parece Vela basin (Tani et al., 2011).

4. Analytical Methods

4.1. Secondary Ion Mass Spectrometry

Isotopic compositions and minor and trace element concentrations in zircons were measured by secondary ion mass spectrometry (SIMS) on the SHRIMP-RG ion microprobe at Stanford University, jointly operated by the U.S. Geological Survey and Stanford University. Cathodoluminescence images were used to guide selection of analysis points. Isotopic ratios and U, Th, and Pb concentrations were measured using a ~20 to 30 μm diameter, 3.5 to 4 nA O_2^- primary beam and data reduction procedures described in Barth and Wooden (2006) using Squid 2.51 (Ludwig, 2009). Ages based on isotopic ratios were standardized against Temora-2 zircon (416.8 Ma; Black et al., 2004). Errors on individual zircon spots are reported at 1 sigma (Table S1). Calculated ages are reported as weighted means with 2 sigma standard error. The grain

mounts were lightly repolished and analyzed for a suite of trace elements by SIMS using a ~15 to 20 μm diameter, 1 to 2 nA O_2^- primary beam, and analytical and data reduction procedures described by Barth and Wooden (2010). Trace element concentrations were standardized against Madagascar Green (MADDER) zircon (Table S2).

4.2. Laser Ablation Mass Spectrometry

Isotopic compositions and trace element concentrations in zircons from Expedition 351 drilling mud were measured by laser ablation inductively-coupled plasma mass spectrometry (LA-ICP-MS) on the Agilent mass spectrometer at the University of Tasmania, using methods described by Meffre et al. (2007). Ages based on isotopic ratios were standardized against 91500 zircon (1062.4 Ma; Wiedenbeck et al., 1995) and trace element concentrations were standardized against NIST 610 glass (Supplementary Information Figure S1; Table S3)

5. Results

5.1. Zircon Geochronology

Zircon is expected to be rare or absent in intraoceanic arcs such as the IBM due to generally high eruption temperatures of typical lavas and low Zr abundances which require low estimated temperatures of zircon saturation. In consideration of this general observation, our sampling tested the feasibility of recovering detrital zircons from arc-proximal volcaniclastic rocks in the intraoceanic arc setting at U1438. Zircon is present, though not abundant. We recovered zircons

from eight of thirty-five processed samples in Unit III (**Figure 2**); no zircons were recovered from our samples of Units II and IV. The zircons are euhedral grains and grain fragments typically <80 μm in long dimension, but rare euhedral prismatic grains up 250 μm in length were recovered.

The U1438 zircons have Eocene to Oligocene Pb/U ages (43 to 27 Ma; **Figure 3**). These ages and their associated trace element compositions are incompatible with drilling contamination but compatible with provenance in the KPR oceanic arc. We tested potential contamination during core recovery by analyzing zircons from the drilling mud used during Expedition 351. This sepiolite-based mud was made up from lacustrine sediments in Nevada, USA; it contains Neogene zircons derived from the volcanic and plutonic rocks of the Death Valley part of the Basin and Range province, as well as older grains from local Mesozoic and Proterozoic crystalline basement rocks (Andrews et al., 2016). Our sepiolite mud sample yielded only a single Oligocene grain and none in the 43 to 27 Ma (Eocene to Oligocene) age range of U1438 zircons. In addition, the majority of U1438 zircons have Th/U ≤0.6 and Yb/Gd >15, which further distinguishes them geochemically from Neogene zircons in the drilling mud that are typically high Th/U (~0.8 to 2.8) and have lower Yb/Gd. We conclude from these data that we recovered zircons that did not result from drilling contamination.

SIMS geochronology of U1438 detrital zircons is based on $^{206}Pb^*/^{238}U$ ages, with radiogenic Pb ($^{206}Pb^*$) being corrected for common Pb using measured $^{207}Pb/^{206}Pb$ (Ireland and Williams, 2003). Calculated $^{207}Pb/^{206}Pb$ or $^{207}Pb/^{235}U$ ages are not presented due to low radiogenic yield from such young zircons and generally low measured U concentrations (80% <100 ppm). We

assume that loss of radiogenic Pb is negligible from these low U zircons. Measured $^{206}Pb^*/^{238}U$ ages increase systematically down-core and there is substantial overlap in age ranges among grains from nearby cores (**Figure 4**). Six of the eight samples show a spread of spot ages in excess of what is expected based on analytical errors alone. We therefore calculated the weighted mean $^{206}Pb^*/^{238}U$ age of the youngest homogeneous population in these sample (<1.6 Ma 2 sigma; 30 to >50% of analyses) as our best estimate of the maximum depositional age of each core. Calculated maximum depositional ages increase from 28.9 ± 0.7 Ma in core D17R at ~364 mbsf near the top of Unit III to 37.2 ± 0.9 Ma from core E18R at just below 1000 mbsf (**Figure 4**; Table S4). We find generally good agreement between these detrital maximum depositional ages and sediment depositional ages calculated from biostratigraphy and magnetostratigraphy of Unit III. Older grains are also present in six of eight samples, typically ranging from 2 to 4 million years older than the youngest population, but as much as 9 million years older in core D53R.

We also attempted to recover zircon from the thinner Paleogene volcaniclastic section at Site 1201; however, we recovered only a single zircon from fifteen processed samples (**Figure 2**). The zircon, from core 36R at ~418 mbsf, yielded a $^{206}Pb^*/^{238}U$ age of 35.0 ± 1.1 Ma. Magnetostratigraphy indicates an age of ~33.0 to 34.5 Ma for this depth interval (Salisbury et al., 2002).

The range of U1438 and 1201 detrital zircon ages overlaps with, but is predominantly older than volcanic rocks recovered from the northern KPR flanking the Amami Sankaku Basin. $^{40}Ar/^{39}Ar$ ages of dredged lavas and shallow core samples from atop the northern KPR, the inferred source

area of U1438 Units II, III and IV volcaniclastic sediments, lie within the narrow range of 28 to 25 Ma, similar to the range of ages of volcanic rocks for the entire KPR (Ishizuka et al., 2011b). These younger whole rock ages of surface lavas confirm that the 43 to 27 Ma zircons in volcaniclastic rocks of the Amami Sankaku Basin record melts formed during initiation and/or constructive phases of KPR volcanoes in the northern Izu-Bonin arc system.

5.2. Zircon Minor and Trace Element Geochemistry

Minor and trace element geochemistry of magmatic zircons provide two key categories of petrologic information that supplements Pb/U geochronologic data. Zircon compositions reflect the magmatic environment at zircon saturation, and melt evolution with continued crystallization toward eruption or complete solidification (Anderson et al., 2008; Walker et al., 2010; Barth and Wooden, 2010; Cooper et al., 2014). Trace element abundances and key trace element ratios in populations of magmatic zircons are also useful for discrimination of the tectonic environment within which a magma system evolves (Grimes et al., 2007; 2015). The geochemistry of detrital magmatic zircons can therefore provide independent information on the compositions and tectonic setting of provenance magmatic rocks and can complement inferences from bulk rock compositions. U1438 detrital zircons are compositionally heterogeneous within and between core samples, providing insights into the magmatic environment and evolution of melt compositional diversity of their magmatic provenance rocks. Zircon compositional diversity at U1438 thus provides an age-controlled record that complements tephra and melt inclusion records of magmatic evolution in the juvenile Izu-Bonin arc (Arculus et al., 1995; Straub et al., 2003, 2015; Brandl et al., 2017).

Detrital zircons from U1438 are solid solutions with Hf abundances primarily between 8000 and 11000 ppm (**Figure 5**) and REE abundances that are strongly heavy REE-enriched (Ce/Yb <0.04) with positive Ce and negative Eu anomalies (0.7 to 0.3). Ce/Yb values are lower than is typical for continental zircon suites but overlap with the range of values observed in zircons from mid-ocean ridges. Titanium, Th and U abundances are crudely positively correlated with Hf, as is typical for suites of zircons from arc plutonic and volcanic rocks. Ti concentrations mostly range between 5 and 35 ppm. Th and U abundances are commonly low (<60 and <100 respectively), at the low end of the range of magmatic zircon values, and Th/U is typically <0.6.

Zircons from the 37.5 Ma tonalite at Komahashi-Daini seamount in the northern KPR have broadly similar ranges of Hf, Ti and REE abundances (**Figure 5**). A well-defined negative correlation is observed between Hf and Eu/Eu* for the tonalite zircons, overlapping with the relatively most fractionated detrital zircons. In comparison, the greater scatter in Hf and Ti abundances and Eu/Eu* suggest that the detrital zircons record growth in melts along multiple evolutionary pathways. Zircons from the 48.5 Ma granodiorite from Minami-Koho seamount are distinctive when compared to the detrital and Komahashi-Daini tonalite zircons, having deeper negative Eu anomalies (~0.2) and low Sc (<40 ppm). Gabbro and plagiogranite from the Parece Vela Basin (Godzilla oceanic core complex) contain zircons with distinctively low Sc, high Nb and deep negative Eu anomalies (0.1 to 0.25) compared to zircons from Amami Sankaku Basin volcaniclastic and KPR intrusive rocks.

6. Discussion

The Eocene through Oligocene volcaniclastic sequence of Units II, III, and IV at U1438 constitute a record of early Izu-Bonin arc evolution, for which the tephra glass record is relatively sparse (Arculus et al., 2015b). The ages of arc-derived zircons from this study provide maximum depositional ages for multiple core intervals within Unit III, in particular improving the temporal resolution in the lower two-thirds of Unit III for which age constraints from paleomagnetic data and fossils are more limited and where diagenetic destruction of primary volcanogenic components is pervasive. Below we discuss how the U1438 detrital zircons as a group record oceanic arc provenance in their trace element compositions, and how these compositions record the evolution of compositional asymmetry in the early Izu-Bonin arc.

6.1. Oceanic Arc Provenance of Detrital Zircon

Trace element compositions of zircon populations can be compared to global oceanic zircon data sets to infer the tectonic setting of the provenance (e.g. Grimes et al., 2007). In this regard zircons from the Izu-Bonin arc provide a critical and previously unavailable primitive oceanic arc end-member of magmatic arc-derived zircons. The depositional setting of Amami Sankaku Basin volcaniclastic rocks at U1438 and the Pb/U ages of zircons establishes a juvenile oceanic arc provenance for detrital zircons in this sequence. Following the methodology of Grimes et al. (2015), linear discriminant analysis of global data sets of multi-element analyses (**Figure 6**) indicates that detrital zircons in U1438 volcaniclastic rocks are largely compositionally distinct from oceanic zircons formed in mid-ocean ridge and intraplate tectonic settings, albeit showing some overlap with the range of mid-ocean ridge zircons, and are also compositionally distinct

when compared with zircons from continental arcs. The discriminant functions describing these distinctions are weighted toward relative differences in Ti, U, Nb, Sc and the middle to heavy REE. Abundances of these elements and key ratios can be used to discriminate populations of zircons from distinctive oceanic tectonic settings and to discriminate first-order differences among arc tectonic settings.

It should be noted first that the oceanic arc field overlaps the mid-ocean ridge field (**Figure 6**). In this analysis the distinction of intraoceanic arc from mid-ocean ridge and continental arc zircons depends strongly on Sc abundances to separate arc-derived from mid-ocean ridge zircons. For most other trace elements and ratios intraoceanic arc zircons lie within the range of mid-ocean ridge zircon compositions or exhibit a transitional signature toward more enriched continental arcs. An example of this tendency is that the mid-ocean ridge zircon array has median values for U/Yb and Th/Yb of 0.07 and 0.04 while median values for the Izu-Bonin arc zircons are 0.12 and 0.06, respectively, lying within the upper part of the mid-ocean ridge array (**Figure 7**). Ce/Yb also shows a transitional signature in REE enrichment from mid-ocean ridge to arc data arrays. Thus the overall compositional signature of intraoceanic arc zircons, when compared to mid-ocean ridges, clearly shows that the melts from which these arc zircons crystallized were produced from comparably depleted sources. While these arc melts are modestly enriched with respect to the bulk mid-ocean ridge composition, this enrichment is not enough to produce zircon compositions that are always distinct from those of mid-ocean ridge zircons.

In a practical sense then, a continuum of zircon compositions is observed from mid-ocean ridges through intraoceanic arc towards a variety of continental arc settings. We illustrate the

differences between these intraoceanic and continental arc zircon suites using ratios of trace elements that are sensitive to slab contributions to arc magmas but minimize the effects of fractionation, following the empirical approach used for volcanic rocks (Pearce, 1982; Pearce and Peate, 1995; Grimes et al., 2015). Nb represents a conservative element in arc systems, as it is conserved in the slab and not transferred to arc melts, and U represents a non-conservative element that records slab contributions to arc magmas. In the Nb/Yb vs. U/Yb diagram (**Figure 8a**) mid-ocean ridge and intraplate zircons define the main oceanic zircon array, reflecting relative mantle source enrichment in both U and Nb. In the context of the oceanic array, zircons from the Godzilla oceanic core complex in the Parece Vela Basin record formation from melts with intermediate enrichment in these elements, consistent with the compositions of Parece-Vela Basin lavas (Hickey-Vargas, 1991). In contrast, U1438 detrital zircons lie mainly within and above the main oceanic zircon array, reflecting modest U enrichment and Nb depletion of the melts from which these zircons formed in comparison to zircons crystallized from melts in mid-ocean ridge and back-arc basin settings. The oceanic arc data define a compact field at U/Yb about 0.05 to 0.25, reflecting a transitional compositional character between mid-ocean ridge zircons and those from modern continental arcs with relatively higher U/Yb (~0.3 to 5.0). The well-known range of lithophile element enrichment among arc suites from distinct arc tectonic settings is illustrated for zircons in the Hf vs. U/Yb diagram (**Figure 8b**). Here the U1438 detrital zircons and zircons from dredge samples of KPR tonalite and granodiorite, originating in a relatively primitive low K oceanic arc system, are significantly less enriched than zircons from medium to high-K continental arcs settings illustrated by zircons from the modern North American Cascades and South American Andes. We conclude that U/Yb in populations of zircons is a sensitive indicator of the non-conservative element enrichment in host arc melts, and

the low U/Yb and Nb/Yb in U1438 zircons is consistent with the juvenile oceanic arc provenance inferred for Unit III.

Low Sc abundances and Sc/REE are typical of zircons from mid-ocean ridge and oceanic intraplate settings, when compared to a global data set of arc-derived zircons (Grimes et al., 2015). U1438 zircons generally have Sc>40 and Sc/Gd>1, typical of arc zircon suites and having limited compositional overlap with mid-ocean ridge zircons (**Figure 9**). Discrimination of oceanic arc-derived zircons from other oceanic zircon sources by Sc/REE may be generally applicable due to the relatively extensive fractionation required to saturate mid-ocean ridge melts in zircon, suggesting that many arc melts are not extensively fractionated at the point of zircon saturation.

6.2. Silicic Melt Provenance of Detrital Zircon

The Izu-Bonin arc, like other intraoceanic arcs, is typified by alkali-poor and relatively low Zr melts and a scarcity of magmatic zircon. Zircon has been reported, however, in several tuffs recovered by Expedition 350 in the proximal Izu-Bonin rear arc (Schmitt et al., in press), in Late Miocene dacite from the Izu Peninsula, and in the 37.5 Ma Komahashi-Daini tonalite (Tani et al., 2010, 2011). The provenance of U1438 detrital zircons in terms of the petrologic character of host melts provides insights into the genesis of Zr-saturated magmas in the Izu-Bonin arc.

Comparison of zircon saturation temperatures of IBM melts with Ti abundances in detrital zircons provides constraints on the temperature and composition of the detrital zircon host melts.

Incompatible alkalis and Zr are concentrated in fractionating melts, yielding progressively higher estimated temperatures for zircon saturation using the silicate melt saturation model of Watson and Harrison (1983; see also Boehnke et al., 2013). Model saturation temperatures for typical IBM low-K arc front lavas are <750°C using this melt model, but model temperatures are as high as ~850°C for medium-K, Zr-richer rear arc lavas (**Figure 10**). Zircon saturation is therefore unlikely in high temperature intermediate to silicic arc-front lavas (900 – 1100°C in silicic andesite to rhyolite; de Moor et al., 2005; Shukuno et al., 2006). Zircon saturation is possible, however, in relatively cooler, hydrous and fractionated silicic lavas and intrusions - particularly those with Zr-enriched rear arc melt compositions. Titanium concentrations in zircons provide model crystallization temperatures that may be compared to these ranges of melt saturation temperatures (Watson et al., 2006). Because the melt sources of the detrital zircons are not known, we calculated model zircon-melt temperatures using the calibration of Ferry and Watson (2007) with a_{SiO2} and a_{TiO2} ranging from 0.7 to 1.0., within the range of calculated titania activities in felsic melts that are consistent with the zircon thermometer (Hayden and Watson, 2007). Maximum temperatures are calculated at the highest Ti abundances and silica activities. Ti abundances in detrital zircons range from 6 to 30 ppm; maximum model temperatures based on these abundances using the thermometer of Ferry and Watson range from ~830 to 870°C, reflecting both a range in Ti abundances and a range in reasonable values for silica activity less than unity (**Figure 10**). Igneous zircons from Komahashi-Daini tonalite yield slightly lower maximum temperature ranges of ~770 to 810°C. These model results support a hypothesis that U1438 detrital zircons were derived from saturated KPR melt hosts with rear arc compositional affinity, melts that were Zr-rich, silicic and relatively cool compared to modern arc front lavas. Dacite tephras in modern arc systems that are zircon-bearing (e.g. Pinatubo, San Pedro, >3000

y.b.p. Mount St. Helens dacites) are medium to high K and yield experimentally-verified temperatures of 780 to 850°C, and these cool silicic melts are characterized by high water contents and oxygen fugacities (NNO +1 to +3; Geschwind and Rutherford, 1992; Gardner et al., 1995; Rutherford and Devine, 1996; Scaillet and Evans, 1999; Costa et al., 2004). The range of model temperatures for Izu-Bonin zircons support a provenance for detrital zircons in such cool and hydrous silicic melts.

Detrital zircon REE abundances suggest growth in melts with flat to slightly REE-enriched compositions, an observation that further supports a rear arc affinity for the host melts. Chondrite-normalized REE abundances of host melts were calculated using dacite-melt partition coefficients, and model average melt REE patters were calculated for each time interval in Unit III from which zircons were recovered (**Figure 11**). Chondrite-normalized model melt compositions have rather flat middle and heavy REE and are modestly light REE-enriched, especially after 35 Ma, with average chondrite-normalized Nd/Yb ~1 to 3. The light REE-enriched model melts are similar to KPR and modern Izu-Bonin rear arc dacites and rhyolites, and to 29 to 30 Ma plagioclase and clinopyroxene-hosted dacitic to rhyolitic melt inclusions from U1438 (Nd/Yb ~1.5 to 2.5; Brandl et al., 2017).

6.3. Juvenile Arc Evolution Recorded in Detrital Zircon Ages and Compositions

Regional turbidite and tephra records for the Izu-Bonin arc system indicate diverse magma types have erupted during initiation and building of the arc, including dacite and rhyolite (Gill et al., 1994; Arculus et al., 1995; Straub, 2003; Straub et al., 2015). The KPR-IBM arc system initiated

by infant arc spreading and eruption of highly depleted arc basalt and boninite above the foundering Pacific Plate from ~52 to 44 Ma (Ishizuka et al., 2006b; Arculus et al., 2015a). Building of the juvenile oceanic arc from ~42 to 28 Ma is recorded by early eruption of low-K, high-Mg andesite, followed by arc tholeiitic basalt and andesite as deep subduction became well established beneath the arc after 37 Ma (Brandl et al., 2017). KPR whole rock data, tephra glasses, and melt inclusions from U1438 volcaniclastic rocks indicate arc asymmetry developed ~37 - 35 Ma with eruption of medium-K rear arc andesite, along with less common dacite and rhyolite (Ishizuka et al., 20011b; Straub et al., 2015; Brandl et al., 2017). Slab rollback and intra-arc rifting beginning ~28 Ma stranded the KPR remnant arc east of the Shikoku and Parece Vela back-arc basins.

At U1438 in the Amami Sankaku Basin, the ~52 to 44 Ma infant arc stage is represented by igneous basement (Unit 1) and overlying clastic rocks of Unit IV and lowermost Unit III. No detrital zircons have yet been recovered from these intervals. However, 51.5 and 46.5 Ma intrusive rocks from Santa Rosa Bank in the Mariana forearc and 48.5 Ma granodiorite from Minami-Koho seamount in the northern KPR yielded magmatic zircons crystallized during the infant arc stage (Ishizuka et al., 2011b; Reagan et al., 2013). Zircons from 51.5 Ma gabbro are compositionally distinctive with a wide range in Hf and deep negative Eu anomalies compared to younger detrital zircons (**Figure 5**). Zircons from the younger (46.5 Ma) Santa Rosa tonalite are compositionally more similar to zircons from younger late Eocene intrusive rocks and to U1438 detrital zircons (M. Reagan, pers. comm., 2017), suggesting crystallization from melts that were not as Zr-depleted and/or extensively fractionated prior to zircon saturation. Although the data are limited in number, these zircons are compositionally transitional between mid-ocean ridge

and magmatic arc in geochemical character and illustrate that zircon compositional data may be able to capture the boninitic infant arc stage of magmatism.

Detrital zircons were recovered from most of Unit III, and their 16 million year age range represents nearly the full inferred duration of the juvenile stage of Izu-Bonin oceanic arc magmatism (Arculus et al., 2015a; **Figure 2**). Ages ranging from 43 to 27 Ma indicate that zircon-saturated melts formed in the KPR arc throughout Unit III time, but our data suggest such melts became progressively more common after 35 Ma, during deposition of the last two coarsening-upward packages generated immediately prior to rifting and demise of the KPR arc. Detrital zircons show significant variations in trace element compositions with time in Unit III (**Figure 12**). Trends in zircon composition are illustrated relative to a baseline zircon compositional group, present throughout, defined by low U concentrations (≤60 ppm). Compared to this baseline low-U trend, zircon compositions became more varied and enriched between about 35 and 30 Ma. These more enriched compositions include especially higher concentrations of lithophile elements U and Th, and light REE. In contrast to these incompatible elements, the more compatible elements Ti and Sc do not show comparable enrichments.

The transition in compositions of detrital zircons at ~35 Ma reflects an increase in the frequency of occurrence of enriched compositions that can be explained by generation of relatively enriched melts of rear arc affinity. There is little evidence that the range of trace element abundances and ratios are primarily controlled by the extent of *in situ* fractionation of the host melts. Although trace element ratios such as U/Yb, Th/U and Ce/Yb show significant increase in average values between 35 and 30 Ma, reflecting Th, U and light REE enrichment, the range and

average Hf solid solution show little change through time (**Figure 12**). This observation suggest that non-conservative, incompatible trace element ratios of the detrital zircons record a shift toward more enriched silicic melt compositions in the early Izu-Bonin arc beginning at about 35 Ma.

The detrital zircon record of juvenile Izu-Bonin silicic magmatism at site U1438 supports and supplements the existing record from whole rock lavas and melt inclusions. The volcanotectonic model of Ishizuka et al. (2011b), based primarily on basalt and andesite whole rock data, suggests that arc asymmetry developed after 40 Ma and persisted until the timing of rifting and demise of the Izu-Bonin (Kyushu-Palau) juvenile arc. Clinopyroxene and plagioclase-hosted melt inclusions from U1438 volcaniclastic rocks are primarily basaltic to andesitic as well, although dacitic to rhyolitic melt inclusions are more abundant in 31 to 29 Ma cores (Brandl et al., 2017). The melt inclusion record indicates diverse melts, some with rear arc affinity, were generated as the juvenile arc evolved after 37 Ma. The temporally well-constrained detrital zircons are consistent with and supplement these data sets, recording generation of variably enriched silicic melts over the ~16 Ma life of this juvenile oceanic arc. The most enriched zircon-saturated melts are evident after 35 Ma, and these zircon data provide support for models of well-developed arc asymmetry from ~35 to 28 Ma that are based on lava and melt inclusion records.

7. Conclusions

Detrital zircons recovered from proximal back-arc volcaniclastic sandstones record infant and juvenile stages of the IBM arc. Pb/U maximum depositional ages reinforce shipboard biostratigraphy and magnetostratigraphy of the volcaniclastic sequence, indicating that zircons were generated in the juvenile arc stage and delivered promptly to the proximal back-arc site of deposition. Trace element abundances and ratios of these zircons have key similarities and differences when compared to regional and global oceanic zircon suites. Detrital zircons span the compositional range between zircons from mid-ocean ridge gabbros and zircons from relatively enriched continental arcs, as predicted for melts in a primitive oceanic arc setting derived from a highly depleted mantle source. Melt zircon saturation temperatures and Ti-in-zircon thermometry suggest a provenance in cool and silicic melts that evolved toward more Th and U-rich compositions after about 35 Ma. These temporal trends in detrital zircon compositions suggest regional arc asymmetry characterized by enriched rear-arc silicic melts developed at this time in the evolutionary history of the juvenile IBM arc.

8. Acknowledgements

Support for this research was provided by the IODP, the United States Implementing Organization, and the U.S. National Science Foundation through grant NSF OCE-1558830 to APB. We thank the Captain and crew of the JOIDES Resolution and shipboard technical staff for their outstanding work on Expedition 351. K. Bogus, K. Marsaglia and I. Savov provided critical advice in sampling, and T. Carley, J. Gill, N. Riggs and A. Schmitt provided enlightening

discussions of these data. We thank M. Reagan and B. McClelland for sharing their unpublished observations from Santa Rosa Bank.

Supporting data are included as supplementary text and data files.

9. References

Anderson, J.L., Barth, A.P., Wooden, J.L., and Mazdab, F., 2008, Thermometers and thermobarometers in granitic systems, in Putirka, K.D., and Tepley, F.J., eds., Minerals, Inclusions and Volcanic Processes: Mineralogical Society of America Reviews in Mineralogy, 69, 121-142.

Andrews, G.D., Schmitt, A.K., Busby, C.J., Brown, S.R., Blum, P. and Harvey, J., 2016, Age and compositional data of zircon from sepiolite drilling mud to identify contamination of ocean drilling samples: Geochem. Geophys. Geosys., 17, 3512-3526.

Arculus, R.J., Gill, J.B., Cambray, H., Chen, W., and Stern, R.J., 1995, Geochemical evolution of arc systems in the western Pacific: the ash and turbidite record recovered by drilling, in Taylor, B., and Natland, J. (eds.), Active Margins and Marginal Basins of the Western Pacific: Amer. Geophys. Union Mon., 88, 45-65.

Arculus, R.J., Ishizuka, O., Bogus, K.A., Gurnis, M.C., Hickey-Vargas, R., Aljahdali, M.H., Bandini, A.N., Barth, A.P., Brandl, P.A., Drab, L., Guerra, R., Hamada, M., Jiang, F., Kanayama, K., Kender, S., Kusano, Y., Li, H., Loudin, L.C., Maffione, M., Marsaglia, K.M., McCarthy, A., Meffre, S., Morris, A., Neuhaus, M., Savov, I.P., Sena, C., Tepley, F.J., van der Land, C., Yogodzinski, G.M., and Zhang, Z., 2015a, A record of spontaneous

subduction initiation in the Izu-Bonin-Mariana arc: Nat. Geosci., 8, 728-733, doi: 10.1038/ngeo2515.

Arculus, R.J., Ishizuka, O., Bogus, K., and the Expedition 351 Scientists, 2015b, Izu-Bonin-Mariana arc origins: continental crust formation at an intra-oceanic arc: foundation, inception, and early evolution: International Ocean Discovery Program Preliminary Report, 351, http://dx.doi.org/10.14379/iodp.pr.351.2015.

Barth, A.P., and Wooden, J.L., 2006, Timing of magmatism following initial convergence at a passive margin, southwestern U.S. Cordillera, and ages of lower crustal magma sources: J. Geol., 114, 231-245.

Barth, A.P., and Wooden, J.L., 2010, Coupled elemental and isotopic analyses of polygenetic zircons from granitic rocks by ion microprobe, with implications for melt evolution and the sources of granitic magmas: Chem. Geol., 277, 149-159.

Barth, A.P., Feilen, A.D.G., Yager, S.L., Douglas, S.R., Wooden, J.L., Riggs, N.R., and Walker, J.D., 2012, Petrogenetic connections between ash-flow tuffs and a granodioritic to granitic intrusive suite in the Sierra Nevada arc, California: Geosphere, 8, 250-264, doi:10.1130/GES00737.1.

Barth, A.P., Wooden, J.L., Jacobson, C.E., and Economos, R.C., 2013, Detrital zircon as a proxy for tracking the magmatic arc system: The California arc example: Geol., 41, 223-226.

Black, L.P., Kamo, S.L., Allen, C.M., Davis, D.W., Aleinikoff, J.N., Valley, J.W., Mundil, R., Campbell, I.H., Korsch, R.J., Williams, I.S., and Foudoulis, C., 2004, Improved 206Pb/238U microprobe geochronology by the monitoring of a trace-element-related matrix effect; SHRIMP, ID–TIMS, ELA–ICP–MS and oxygen isotope documentation for a series of zircon standards: Chem. Geol., 205, 115-140.

Boehnke, P., Watson, E.B., Trail, D., Harrison, T.M., and Schmitt, A.K., 2013, Zircon saturation re-revisited: Chem. Geol., 351, 324-334.

Brandl, P.A., Hamada, M., Arculus, R.J., Johnson, K., Marsaglia, K.M., Savov, I.P., Ishizuka, O., and Li, H., 2017, The arc arises: The links between volcanic output, arc evolution and melt composition: Earth Planet. Sci. Lett., 461, 73-84, 10.1016/j.epsl.2016.12.027.

Carley, T.L., Miller, C.F., Wooden, J.L., Bindeman, I.N. and Barth, A.P., 2011, Zircon from historic eruptions in Iceland: reconstructing storage and evolution of silicic magmas: Mineral. Petrol., 102, 135-161.

Claiborne, L.L., 2011, Understanding upper crustal silicic magmatic systems using the temporal, compositional and thermal record in zircon [Ph.D. Dissertation]: Nashville, Vanderbilt University, 375 pp.

Cooper, G.F., Wilson, C.J., Charlier, B.L., Wooden, J.L., and Ireland, T.R., 2014, Temporal evolution and compositional signatures of two supervolcanic systems recorded in zircons from Mangakino volcanic centre, New Zealand: Contrib. Mineral. Petrol., 167, 1-23.

Costa, F., Scaillet, B., and Pichavant, M., 2004, Petrological and experimental constraints on the pre-eruption conditions of Holocene dacite from Volcan San Pedro (36°S, Chilean Andes) and the importance of sulphur in silicic subduction-related magmas: J. Petrol., 45, 855-881.

de Moor, J.M., Fischer, T.P., Hilton, D.R., Hauri, E., Jaffe, L.A. and Camacho, J.T., 2005, Degassing at Anatahan volcano during the May 2003 eruption: implications from petrology, ash leachates, and SO_2 emissions: J. Volc. Geotherm. Res., 146, 117-138.

Dickinson, W.R., 1974, Sedimentation within and beside ancient and modern magmatic arcs, in Dott, R.H. (ed.), Modern and Ancient Geosynclinal Sedimentation: SEPM Spec. Pub. 19, 230-239.

Dickinson, W.R., 1982, Compositions of sandstones in circum-Pacific subduction complexes and fore-arc basins: Amer. Assoc. Petrol. Geol. Bull., 66, 121-137.

Dilles, J.H., Kent, A.J., Wooden, J.L., Tosdal, R.M., Koleszar, A., Lee, R.G. and Farmer, L.P., 2015, Zircon compositional evidence for sulfur-degassing from ore-forming arc magmas: Econ. Geol., 110, 241-251.

Draut, A.E., and Clift, P.D., 2006, Sedimentary processes in modern and ancient oceanic arc settings; evidence from the Jurassic Talkeetna Formation of Alaska and the Mariana and Tonga arcs, western Pacific: J. Sed. Res., 76, 493-514.

Draut, A.E., and Clift, P.D., 2013, Differential preservation in the geologic record of intraoceanic arc sedimentary and tectonic processes: Earth Sci. Rev., 116, 57-84.

Ferry, J.M., and Watson, E.B., 2007, New thermodynamic models and revised calibrations for the Ti-in-zircon and Zr-in-rutile thermometers: Contrib. Mineral. Petrol., 154, 429-437.

Gardner, J.E., Rutherford, M., Carey, S., and Sigurdsson, H., 1995, Experimental constraints on pre-eruptive water contents and changing magma storage prior to explosive eruptions of Mount St Helens volcano: Bull. Volc, 57, 1-17.

Geschwind, C., and Rutherford, M.J., 1992, Cummingtonite and the evolution of the Mount St. Helens (Washington) magma system: An experimental study: Geol., 20, 1011-1014.

Gill, J.B., 1981, Orogenic Andesites and Plate Tectonics: Berlin, Springer Verlag, 390p.

Gill, J.B., Hiscott, R.N., and Vidal, P., 1994, Turbidite geochemistry and evolution of the Izu-Bonin arc and continents: Lithos, 33, 135-168.

Grimes, C.B., John, B.E., Kelemen, P.B., Mazdab, F.K., Wooden, J.L., Cheadle, M.J., Hanghøj, K., and Schwartz, J.J., 2007, Trace element chemistry of zircons from oceanic crust: A method for distinguishing detrital zircon provenance: Geol., 35, 643-646.

Grimes, C.B., John, B.E., Cheadle, M.J., Mazdab, F.K., Wooden, J.L., Swapp, S., and Schwartz, J.J., 2009, On the occurrence, trace element geochemistry, and crystallization history of zircon from in situ ocean lithosphere: Contrib. Mineral. Petrol., 158, 757-783.

Grimes, C.B., Wooden, J.L., Cheadle, M.J., and John, B.E., 2015, "Fingerprinting" tectono-magmatic provenance using trace elements in igneous zircon: Contrib. Mineral Petrol, 170, 46.

Hayden, L.A., and Watson, E.B., 2007, Rutile saturation in hydrous siliceous melts and its bearing on Ti-thermometry of quartz and zircon: Earth Planet. Sci. Lett., 258, 561-568.

Haraguchi, S., Ishii, T., Kimura, J., and Ohara, Y., 2003, Formation of tonalite from basaltic magma at the Komahashi-Daini Seamount, northern Kyushu-Palau Ridge in the Philippine Sea, and growth of Izu-Ogasawara (Bonin)-Mariana arc crust: Contrib. Mineral. Petrol., 145, 151-168.

Haraguchi, S., Ishii, T., Kimura, J., and Kato, Y., 2012, The early Miocene (~25 Ma) volcanism in the northern Kyushu-Palau Ridge, enriched mantle source injection during rifting prior to the Shikoku backarc basin opening: Contrib. Mineral. Petrol., 163, 483-504.

Hickey-Vargas, R., 1991, Isotope characteristics of submarine lavas from the Philippine Sea: implications for the origin of arc and basin magmas of the Philippine tectonic plate: Earth Planet. Sci. Lett., 107, 290-304.

Hochstaedter, A.G., Gill, J.B., Taylor, B., Ishizuka, O., Yuasa, M., and Morita, S., 2000, Across-arc geochemical trends in the Izu-Bonin arc: constraints on source composition and mantle melting: J. Geophys. Res. B, 105, 495-512.

Hochstaedter, A., Gill, J., Peters, R., Broughton, P., Holden, P., and Taylor, B., 2001, Across-arc geochemical trends in the Izu-Bonin arc: contributions from the subducting slab: Geochem., Geophys., Geosyst., 2, doi: 10.1029/2000GC000105.

Ireland, T.R., and Williams, I.S., 2003, Considerations in zircon geochronology by SIMS: Reviews in Mineralogy and Geochemistry, 53, 215-241.

Ishizuka, O., Taylor, R.N., Milton, J.A., and Nesbitt, R.W., 2003, Fluid-mantle interaction in an intra-oceanic arc: constraints from high-precision Pb isotopes: Earth Planet. Sci. Lett., 211, 221-236.

Ishizuka, O., Taylor, R.N., Milton J.A., Nesbitt, R.W., Yuasa, M., and Sakamoto, I., 2006a, Variation in the source mantle of the northern Izu arc with time and space - Constraints from high-precision Pb isotopes: J. Volc. Geotherm. Res., 156, 266-290.

Ishizuka, O., Kimura, J., Li, Y.B., Stern, R.J., Reagan, M.K., Taylor, R.N., Ohara, Y., Bloomer, S.H., Ishii, T., Hargrove, U.S., and Haraguchi, S., 2006b, Early stages in the evolution of Izu–Bonin arc volcanism: New age, chemical, and isotopic constraints: Earth Planet. Sci. Lett., 250, 385-401.

Ishizuka, O., Tani, K., Reagan, M.K., Kanayama, K., Umino, S., Harigane, Y., Sakamoto, I., Miyajima, Y., Yuasa, M., and Dunkley, D.J., 2011a, The timescales of subduction initiation and subsequent evolution of an oceanic island arc: Earth Planet. Sci. Lett., 306, 229-240.

Ishizuka, O., Taylor, R.N., Yuasa, M., and Ohara, Y., 2011b, Making and breaking an island arc: a new perspective from the Oligocene Kyushu-Palau arc, Philippine Sea: Geochem., Geophys., Geosyst., 12, doi: 10.1029/2010GC003440.

Kern, J.M., de Silva, S.L., Schmitt, A.K., Kaiser, J.F., Iriarte, A.R., and Economos, R., 2016, Geochronological imaging of an episodically constructed subvolcanic batholith: U-Pb in

zircon chronochemistry of the Altiplano-Puna Volcanic Complex of the Central Andes: Geosphere, 12, 1054-1077.

Kimura, J.-I., Kent, A.J.R., Rowe, M.C., Katakuse, M., Nakano, F., Hacker, B.R., van Keken, P.E., Kawabata, H., and Stern, R.J., 2010, Origin of cross-chain geochemical variation in Quaternary lavas from the northern Izu arc: Using a quantitative mass balance approach to identify mantle sources and mantle wedge processes: Geochem. Geophys. Geosyst., 11, Q10011, doi:10.1029/2010GC003050.

Kitajima K, Takahata N., and Sano, Y., 2009, Determination of zircon/melt REE partition coefficient from 7μm spot analysis using NanoSIMS: Geochim. Cosmochim. Acta, 73 Supplement, A664.

Kodaira, A., Sato, T., Takahashi, N., Miura, S., Tamura, Y., Tatsumi, Y., and Kaneda, Y., 2007, New seismological constraints on growth of continental crust in the Izu-Bonin intra-oceanic arc: Geol., 35, 1031-1034.

Ludwig, K.R., 2009, Squid 2, A user's manual, Berkeley Geochronology Center Special Publication No. 5, p. 110.

Meffre, S., Scott, R.J., Glen, R.A. and Squire, R.J., 2007, Re-evaluation of contact relationships between Ordovician volcanic belts and the quartz-rich turbidites of the Lachlan Orogen: Aus. J. Earth Sci., 54, 363-383.

Nishizawa, A., Kaneda, K., and Katagiri, Y., 2007, Variation in crustal structure along the Kyushu-Palau Ridge at 15-21N on the Philippine Sea plate based on seismic refraction profiles: Earth Planets Space, 59, e17-e20.

Pearce, J.A., 1982, Trace element characteristics of lavas from destructive plate boundaries, in Thorpe, R.S., ed., Andesites: Orogenic Andesites and Related Rocks: Chichester, John Wiley and Sons, p. 525-548.

Pearce, J.A., and Peate, D.W., 1995, Tectonic implications of the composition of volcanic arc magmas: Ann. Rev. Earth Planet. Sci., 23, 251-285.

Reagan, M.K., McClelland, W.C., Girard, G., Goff, K.R., Peate, D.W., Ohara, Y. and Stern, R.J., 2013, The geology of the southern Mariana fore-arc crust: Implications for the scale of Eocene volcanism in the western Pacific: Earth Planet. Sci. Lett., 380, 41-51.

Rudnick, R.L., and Gao, S., 2004, Composition of the continental crust: Treatise in Geochemistry, 3, 1-64.

Rutherford, M.J., and Devine, J.D., 1996, Preeruption pressure-temperature conditions and volatiles in the 1991 dacite magma of Mount Pinatubo, in Newhall, C.G., and Punongbayan, R.S., eds., Fire and Mud: Eruptions and Lahars of Mount Pinatubo: Seattle, University of Washington Press, 751-766.

Salisbury, M.H., Shinohara, M., Richter, C., et al., 2002, Proceedings of the Ocean Drilling Program, Initial Reports 195: College Station, TX (Ocean Drilling Program), doi:10.2973/odp.proc.ir.195.2002

Salisbury, M.H., Shinohara, M., Suetsugu, D., Arisaka, M., Diekmann, B., Januszczak, N., and Savov, I.P., 2006, Leg 195 synthesis: Site 1201 - a geological and geophysical section in the West Philippine Basin from the 660-km discontinuity to the mudline, in Shinohara, M., Salisbury, M.H., and Richter, C. (eds.), Proc. ODP, Sci. Results, 195: College Station, TX (Ocean Drilling Program), doi:10.2973/odp.proc.sr.195.113.2006.

Sano, Y., Terada, K., and Fukuoka, T., 2002, High mass resolution ion microprobe analysis of rare earth elements in silicate glass, apatite and zircon: lack of matrix dependency: Chem. Geol., 184, 217-230.

Scaillet, B., and Evans, B.W., 1999, The 15 June 1991 eruption of Mount Pinatubo. 1. Phase equilibria and pre-eruption P-T-fO2-fH2O condition of the dacite magma: J. Petrol., 40, 381-411.

Schmitt, A.K., Konrad, K., Andrews, G.D.M., Horie, K., Brown, S.R., Koppers, A.A., Pecha, M., Busby, C.J., and Tamura, Y., 2017, 40Ar/39Ar ages and zircon petrochronology for the rear of the Izu-Bonin-Marianas intra-oceanic subduction zone: International Geology Review, doi:10.1080/00206814.2017.1363675.

Shukuno, H., Tamura, Y., Tani, K., Chang, Q., Suzuki,T., and Fiske, R.S., 2006, Origin of silicic magmas and the compositional gap at Sumisu submarine caldera, Izu-Bonin arc, Japan: J. Volc. Geotherm. Res., 156, 187-216.

Stern, R.J., 2004, Subduction initiation: spontaneous and induced: Earth Planet. Sci. Lett., 226, 275-292.

Straub, S.M., 2003, The evolution of the Izu Bonin-Mariana volcanic arcs (NW Pacific) in terms of major elements: Geochem., Geophys., Geosyst. 4, doi:10.1029/2002GC000357.

Straub, S.M., Woodhead, J.D., and Arculus, R.J., 2015, Temporal evolution of the Mariana arc: Mantle wedge and subducted slab controls revealed with a tephra perspective: J. Petrol., 56, 409-439, doi: 10.1093/petrology/egv005.

Takahashi, N., Kodaira, S., and Klemperer, S., Tatsumi, Y., Kaneda, Y., and Suyehiro, K., 2007, Crustal structure and evolution of the Mariana intra-oceanic island arc: Geol., 35, 203-206.

Takahashi, N., Kodaira, S, and Tatsumi, Y., Kaneda, Y., and Suyehiro, K., 2008, Structure and growth of the Izu-Bonin-Mariana arc crust: 1. Seismic constraint on crust and mantle structure of the Mariana arc–back-arc system: J. Geophys. Res., 113:doi:10.1029/2007JB005120.

Takahashi, N., Kodaira, S, and Tatsumi, Y., 2009, Structural variations of arc crusts and rifted margins in the southern Izu-Ogasawara arc-back arc system: Geochem., Geophys., Geosyst., 10:doi:10.1029/2008GC002146.

Tamura, Y., Gill, J.B., Tollstrup, D., Kawabata, H., Shukuno, H., Chang, Q., Miyazaki, T., Takahashi, T., Hirahara, Y., Kodaira, S., Ishizuka, O., Suzuki, T., Kido, Y., Fiske, R.S., and Tatsumi, Y., 2009, Silicic magmas in the Izu-Bonin oceanic arc and implications for crustal evolution: J. Petrol., 50, 685-723.

Tamura, Y., Ishizuka, O., Aoike, K., Kawate, S., Kawabata, H., Chang, Q., Saito, S., Tatsumi, Y., Arima, M., Takahashi, M., Kanamaru, T., Kodaira, S., and Fiske, R.S., 2010, Missing Oligocene crust of the Izu-Bonin arc: Consumed or rejuvenated during collision?: J. Petrol., 51, 823-846.

Tamura, Y., Busby, C., and Blum, P., 2013. Izu-Bonin-Mariana rear arc: the missing half of the subduction factory. IODP Sci. Prosp., 350:doi:10.2204/iodp.sp.350.2013.

Tani, K., Fiske, R.S., Tamura, Y., Kido, Y., Naka, J., Shukuno, H., and Takeuchi, R., 2008, Sumisu volcano, Izu-Bonin arc, Japan: site of a silicic caldera-forming eruption from a small open-ocean island: Bull. Volc., 70, 547-562.

Tani, K., Dunkley, D.J., Kimura, J., Wysoczanski, R.J., Yamada, K., and Tatsumi, Y., 2010, Syncollisional rapid granitic magma formation in an arc-arc collision zone: Evidence from the Tanzawa plutonic complex, Japan: Geol., 38, 215-218.

Tani, K., Fiske, R.S., Dunkley, D.J., Ishizuka, O., Oikawa, T., Isobe, I., and Tatsumi, Y, 2011, The Izu Peninsula, Japan: Zircon geochronology reveals a record of intra-oceanic rear-arc magmatism in an accreted block of Izu–Bonin upper crust: Earth Planet. Sci. Lett., 303, 225-239.

Tani, K., Dunkley, D.J., Chang, Q., Nichols, A.R., Shukuno, H., Hirahara, Y., Ishizuka, O., Arima, M., and Tatsumi, Y., 2015, Pliocene granodioritic knoll with continental crust affinities discovered in the intra-oceanic Izu-Bonin-Mariana Arc: Syntectonic granitic crust formation during back-arc rifting: Earth Planet. Sci. Lett., 424, 84-94.

Taylor, S.R., 1967, The origin and growth of continents: Tectonophys., 4, 17-34.

Tani, K., Dunkley, D.J., and Ohara, Y., 2011b, Termination of backarc spreading: Zircon dating of a giant oceanic core complex: Geol., 39, 47-50.

Tollstrup, D., Gill, J., Kent, A., Prinkey, D., Williams, R., Tamura, Y., and Ishizuka, O., 2010, Across-arc geochemical trends in the Izu-Bonin arc: Contributions from the subducting slab, revisited: Geochem., Geophys., Geosyst., 11:doi: 10.1029/2009GC002847

Wade, J.A., Plank, T., Stern, R.J., Tollstrup, D.L., Gill, J.B., O'Leary, J.C., and Hilton, D.R., 2005, The May 2003 eruption of Anatahan volcano, Mariana Islands: Geochemical evolution of a silicic island-arc volcano: J. Volc. Geotherm. Res., 146, 139-170.

Walker, B.A., Grunder, A.L., and Wooden, J.L., 2010, Organization and thermal maturation of long-lived arc systems: Evidence from zircons at the Aucanquilcha volcanic cluster, northern Chile: Geol., 38, 1007-1010.

Watanabe, S., Widom, E., Ui, T., Miyaji, N., and Roberts, A.M., 2006, The evolution of a chemically zoned magma chamber: The 1707 eruption of Fuji volcano, Japan: J. Volc. Geotherm. Res., 152, 1-19.

Watson, E.B., Wark, D.A., and Thomas, J.B., 2006, Crystallization thermometers for zircon and rutile: Contrib. Mineral. Pet., 151, 413-433.

Watson, E.B., and Harrison, T.M., 1983, Zircon saturation revisited - temperature and composition effects in a variety of crustal magma types: Earth Planet. Sci. Lett., 64, 295-304.

Wiedenbeck, M., Alle, P., Corfu, F., Griffin, W.L., Meier, M., Oberli, F., Vonquadt, A., Roddick, J.C., and Speigel, W., 1995, Three natural zircon standards for U–Th–Pb, Lu–Hf, trace-element and REE analyses: Geostandards News., 19, 1-23

Yoshimoto, M., Fujii, T., Kaneko, T., Yasuda, A., Nakada, S., and Matsumoto, A., 2010, Evolution of Mount Fuji, Japan: Inference from drilling into the subaerial oldest volcano, pre-Komitake: Isl. Arc, 19, 470-488.

Figure 1. Bathymetric map of the eastern Philippine Sea, including the active Izu-Bonin and Mariana arcs - the western Pacific plate is subducting beneath the active arcs. The Kyushu-Palau Ridge is a 50 to 25 Ma remnant arc, separated from the active arcs by spreading between about 25 and 15 Ma in the Shikoku and Parece Vela basins. White stars are IODP Project IBM sites, and numbered dots are other DSDP and ODP sites. Inset map shows detailed bathymetry of the northern Kyushu-Palau Ridge in the vicinity of Site 351-U1438. Red boxes show the location and $^{40}Ar/^{39}Ar$ ages (in Ma) of dredge samples from the northern Kyushu-Palau Ridge (Ishizuka et al., 2011b).

Figure 2. Graphic lithologic logs for IODP Site 1438 (Arculus et al., 2015a) drilled on Expedition 351 in the proximal back-arc of the northern Kyushu-Palau Ridge, and the thinner

section recovered at ODP Site 1201 to the south (Salisbury et al., 2006). See **Figure 1** for locations. On the site columns, open symbols are drill core samples that did not yield zircon, and filled symbols yielded one or more detrital zircons.

Figure 3. Probability plot of $^{206}Pb^*/^{238}U$ ages of detrital zircons from Site U1438 (green) compared to zircons recovered from Expedition 351 drilling mud (grey). Approximately a third of the zircons from the drilling mud yielded Late Archean or Proterozoic ages. Inset graph compares trace element compositions of detrital zircons and Neogene zircons from drilling mud; note that, in addition to age differences, the high average Th/U and low Yb/Gd of the drilling mud zircons are distinctive.

Figure 4. Detrital zircon ages for Unit III volcaniclastic rocks at Site U1438. Left panel shows core numbers and zircon ages vs. depth (in meters below sea floor). Colored bars show $^{206}Pb^*/^{238}U$ age (± 1 sigma) of individual zircon spots, with some shifted slightly in depth for clarity. Grey shaded symbols are zircons older than the youngest population and these were excluded from age calculations. Right panel shows maximum depositional age of the youngest population in each core (± 2 sigma; Table S4); shipboard bio- and magnetostratigraphic estimates of sediment depositional age versus core depth are from Arculus et al. (2015a). Note that zircon maximum depositional ages are in agreement with stratigraphic age estimates.

Figure 5. Covariation of Hf and Ti abundances and the Eu anomaly in U1438 detrital zircons, compared to monogenetic zircon suites from IBM granitic rocks. Note that detrital zircons extend to higher Ti and Eu/Eu* over similar Hf concentration ranges, with greater scatter than observed in most zircon suites from granitic rocks. Data sources for IBM granitic rocks: Santa Rosa Bank, southern Mariana forearc, 51.5 Ma gabbro from Reagan et al. (2013), 48.5 Ma Koho granodiorite and 37.5 Ma Komahashi tonalite from the Kyushu – Palau Ridge (this study).

Figure 6. Linear discriminant analysis of Kyushu-Palau Ridge oceanic arc detrital zircons in comparison to zircons from mid-ocean ridges (Grimes et al., 2009, 2015), Iceland (Carley et al., 2011) and the Sierra Nevada continental arc (Barth et al., 2012; Wooden and Barth, unpub. data). LD1 and LD2 are the first and second linear discriminants.

Figure 7. A) U/Yb vs Th/Yb and B) Ce/Yb vs. Th/Yb diagrams illustrating compositional range of arc zircons relative to zircons from mid-ocean ridges. Data sources: mid-ocean ridge zircons from Grimes et al., (2009), Mt. St. Helens in the modern Cascades from Claiborne (2011), Yanacocha in the Andean Northern Volcanic Zone (Andes NVZ) from Dilles et al. (2015).

Figure 8. A) Nb/Yb vs. U/Yb diagram illustrating slab-related non-conservative behavior of arc-derived zircons relative to non-slab-related mantle enrichment defined by zircons from mid-ocean ridge (MOR), Parece Vela Basin, and oceanic intraplate (OI) settings. Main MOR – OI array is based on mid-ocean ridge zircons from the Mid-Atlantic and Indian ridges (Grimes et al., 2009) and ocean island zircons from Iceland (Carley et al., 2011). Equations of the bounding lines for the main MOR-OI array are $U/Yb = 1.2*(Nb/Yb^{0.8})$ and $U/Yb = 9.0*(Nb/Yb^{0.8})$. Oceanic arc zircons from U1438 detrital suite and KPR granitic rocks (this study) compared to arc zircons from the modern Cascades and Andes NVZ (data sources as in **Figure 7)**. B) Uranium enrichment in arc zircons. The well-known lithophile element enrichment of arc lavas from convergent margin settings is also reflected in relative U enrichment in zircons, where low to high U/Yb zircons are formed in low to high K arc settings. Equations of the bounding lines are U/Yb = 0.0023*e^(0.00034*Hf), U/Yb = 0.0095*e^(0.00034*Hf) and U/Yb = 0.038*e^(0.00033*Hf).

Figure 9. Scandium enrichment in arc zircons compared to mid-ocean ridge and Parece Vela Basin zircons. Symbols and data sources as in **Figure 8**, and mid-ocean ridge data are from

Grimes et al. (2009). Equation for the dividing line separating the main MOR and arc zircon arrays is $Sc/Gd = 81.6*(Yb^{-0.6})$.

Figure 10. Rayleigh fractional crystallization models for IBM arc melts showing zircon saturation temperature with increasing silica, using the silicate melt saturation model of Watson and Harrison (1983). Data sources for lavas: IB arc front (Tamura et al., 2009; Shukuno et al., 2006; Tani et al., 2008), IB rear arc (Hochstaedter et al., 2000, 2001; Tollstrup et al., 2010), Fuji (Watanbe et al., 2006; Yoshimoto et al., 2010), Kyushu-Palau Ridge remnant arc (Ishizuka et al., 2011b; Haraguchi et al., 2012), and Anatahan (Wade et al., 2005). Data source for tonalite is Haraguchi et al. (2003). For comparison, histograms at right show thermometry of IBM zircons for $a_{SiO2} = 1$, using the Ti thermometer of Ferry and Watson (2007). Shaded bars show range of maximum crystallization temperatures at constant titania but varying model silica activities, reflecting uncertainty in whether melts were quartz-saturated. Detrital zircons from U1438 and magmatic zircons from Komahashi-Daini tonalite yield maximum model temperatures of ~830 to 870°C and ~770 to 810°C respectively, at melt silica activities varying from 0.7 to 1.0.

Figure 11. Model chondrite-normalized REE compositions of host melts for U1438 detrital zircons, based on dacite-melt partition coefficients of Sano et al. (2002) and Kitajima et al. (2009). Patterns for arc front dacite whole rock (Shukuno et al., 2006) and light REE-enriched rear arc dacite whole rock (Ishizuka et al., 2011b) are shown for comparison. Most U1438 model host melts are light REE-enriched, although limited data from 37 Ma zircon suggest an overall flat to slightly light REE-depleted melt pattern.

Figure 12. Temporal trends in lithophile and high field strength abundances and REE ratios in detrital zircons from U1438 Unit III. Lighter and darker-shaded zircons represent low and high U groups respectively, and green line indicates a baseline, low U and Th trend through time. Note

that there is no difference between the two groups in terms of average Hf or Ti concentrations or average REE fractionation, but that the high U and Th group has higher average U/Yb and Th/U.

Figure 1.

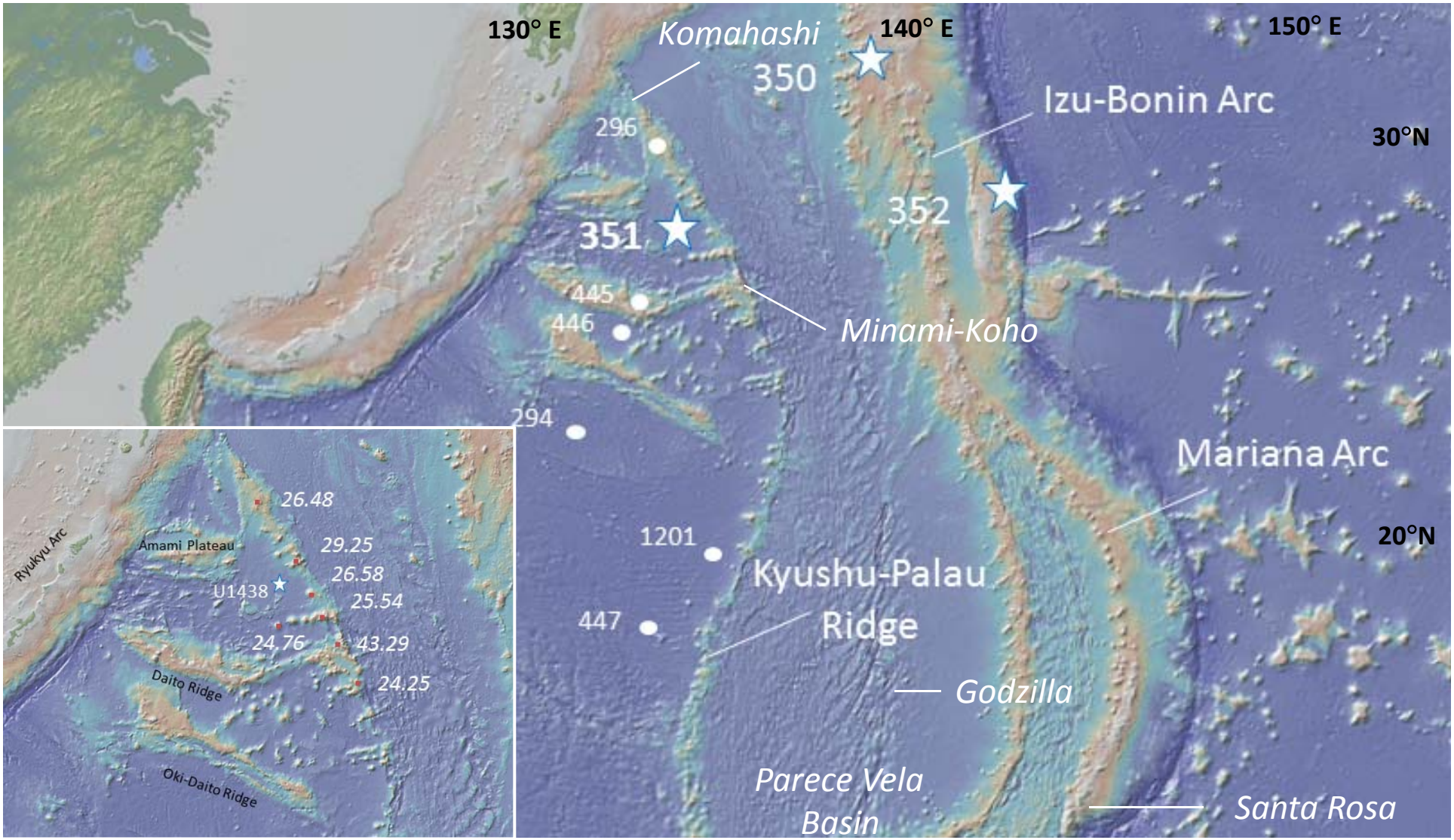

Figure 2.

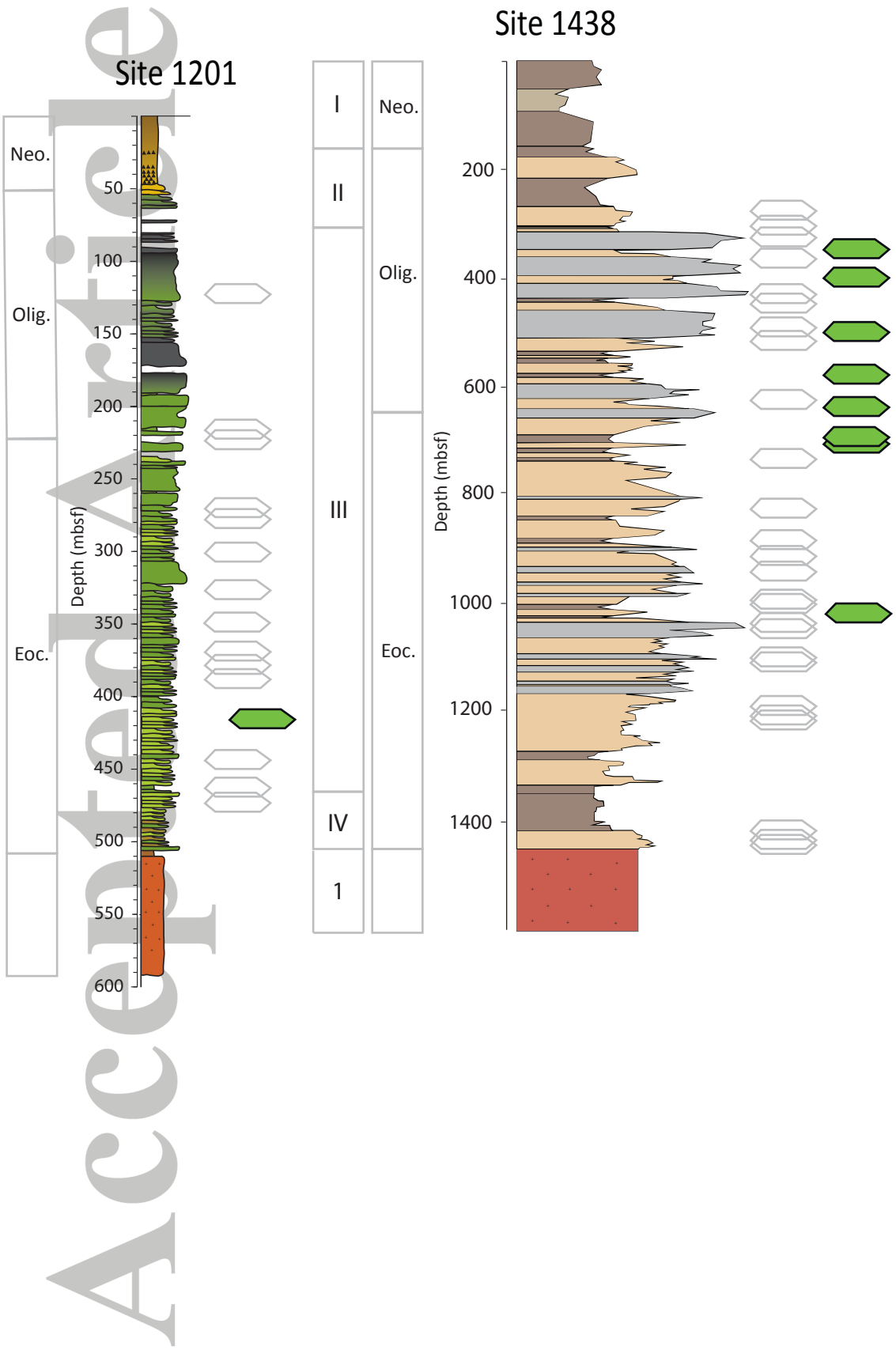

Figure 3.

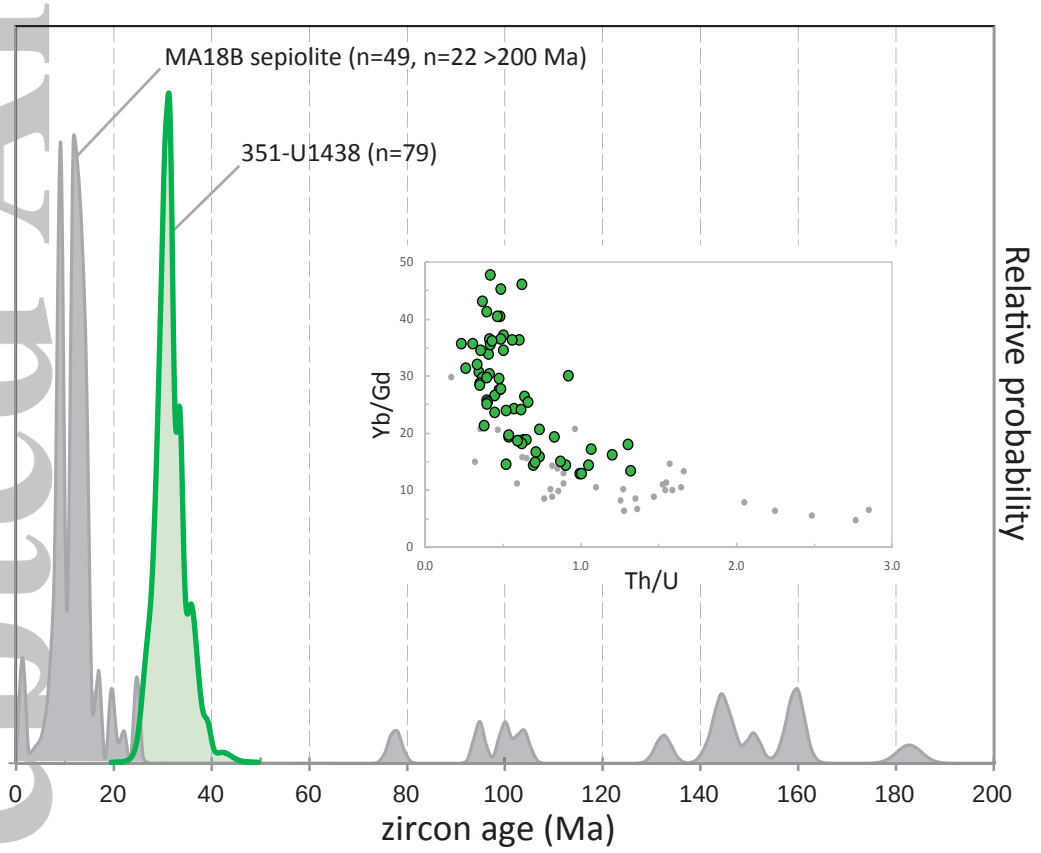

Figure 4.

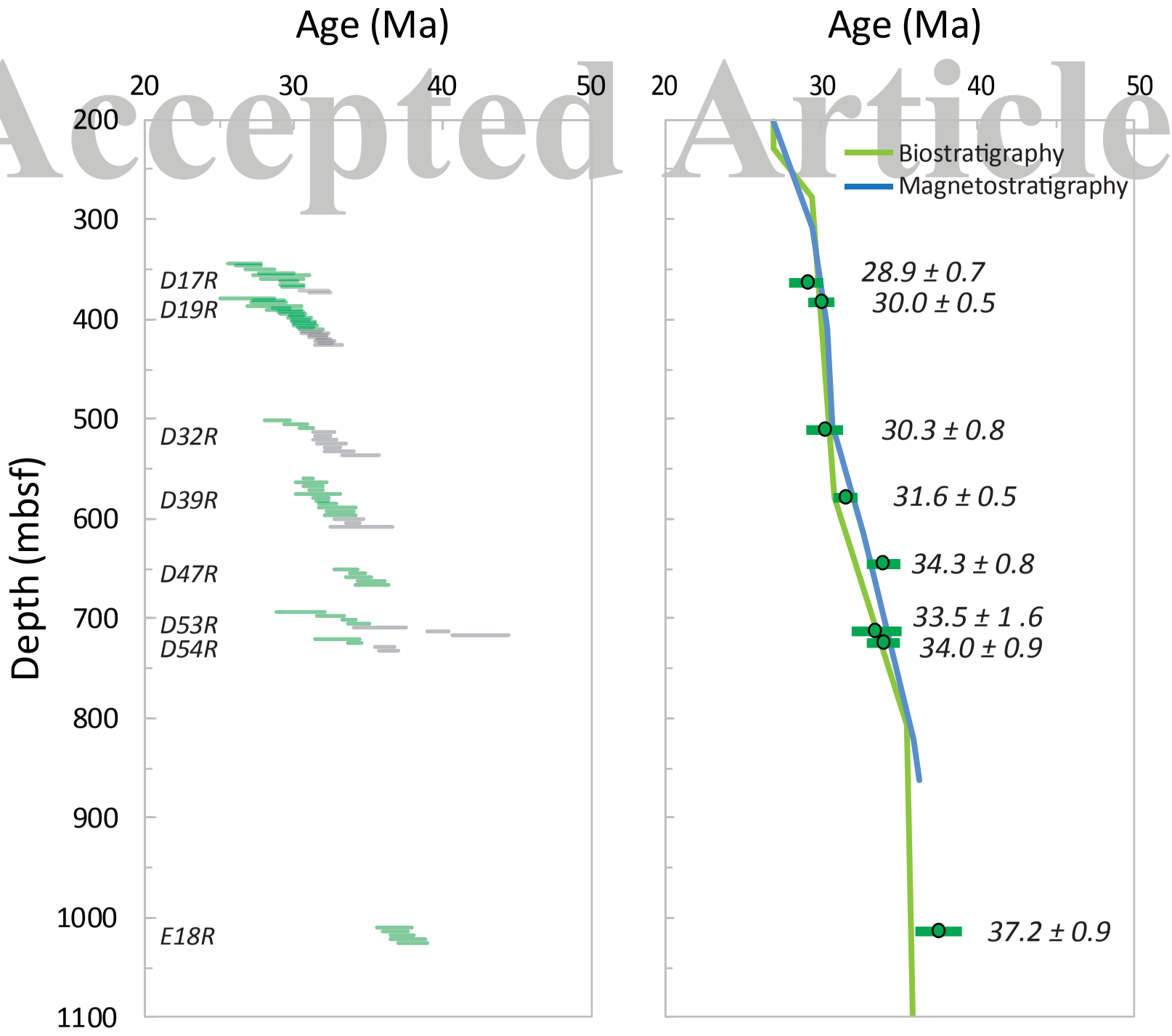

Figure 5.

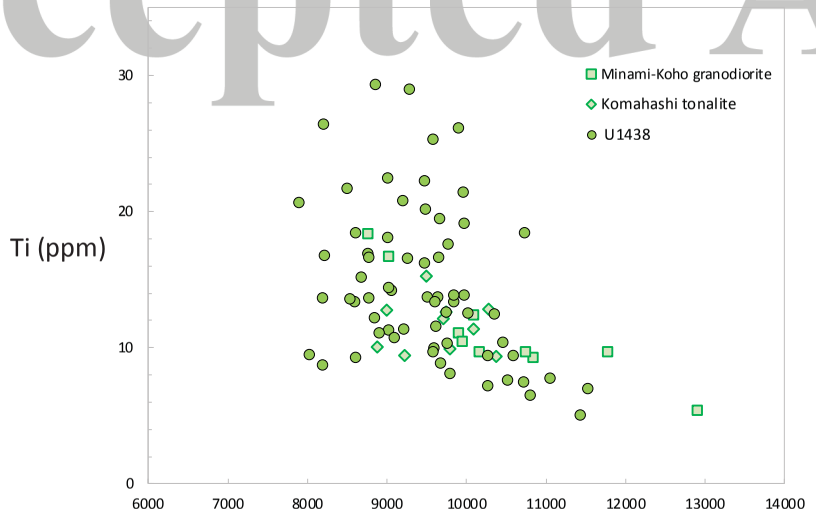

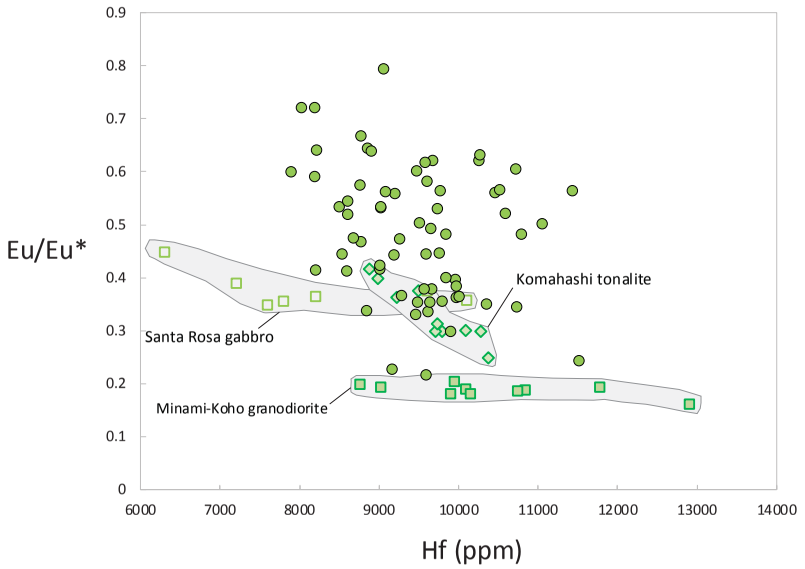

Figure 6.

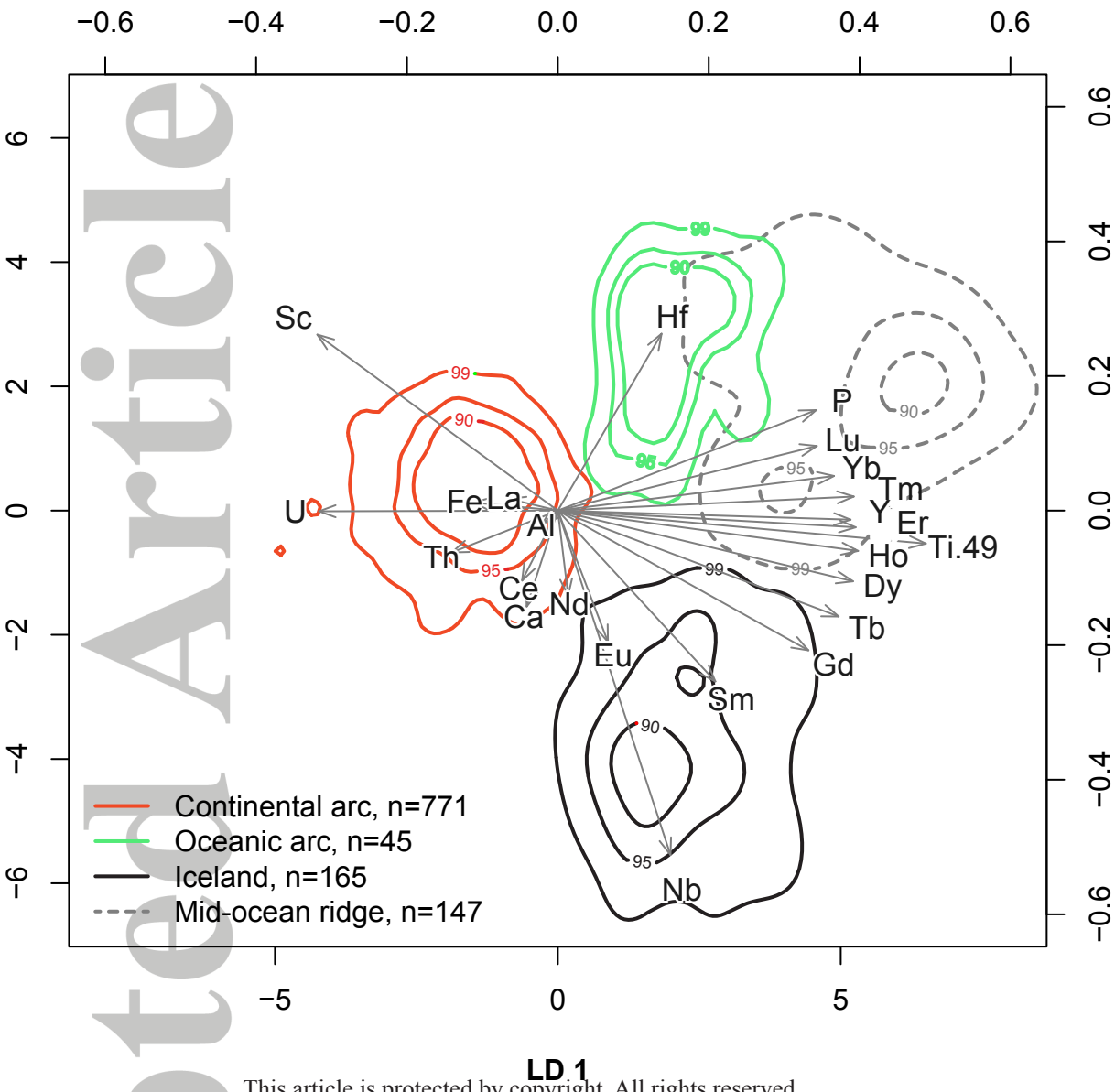

Figure 7.

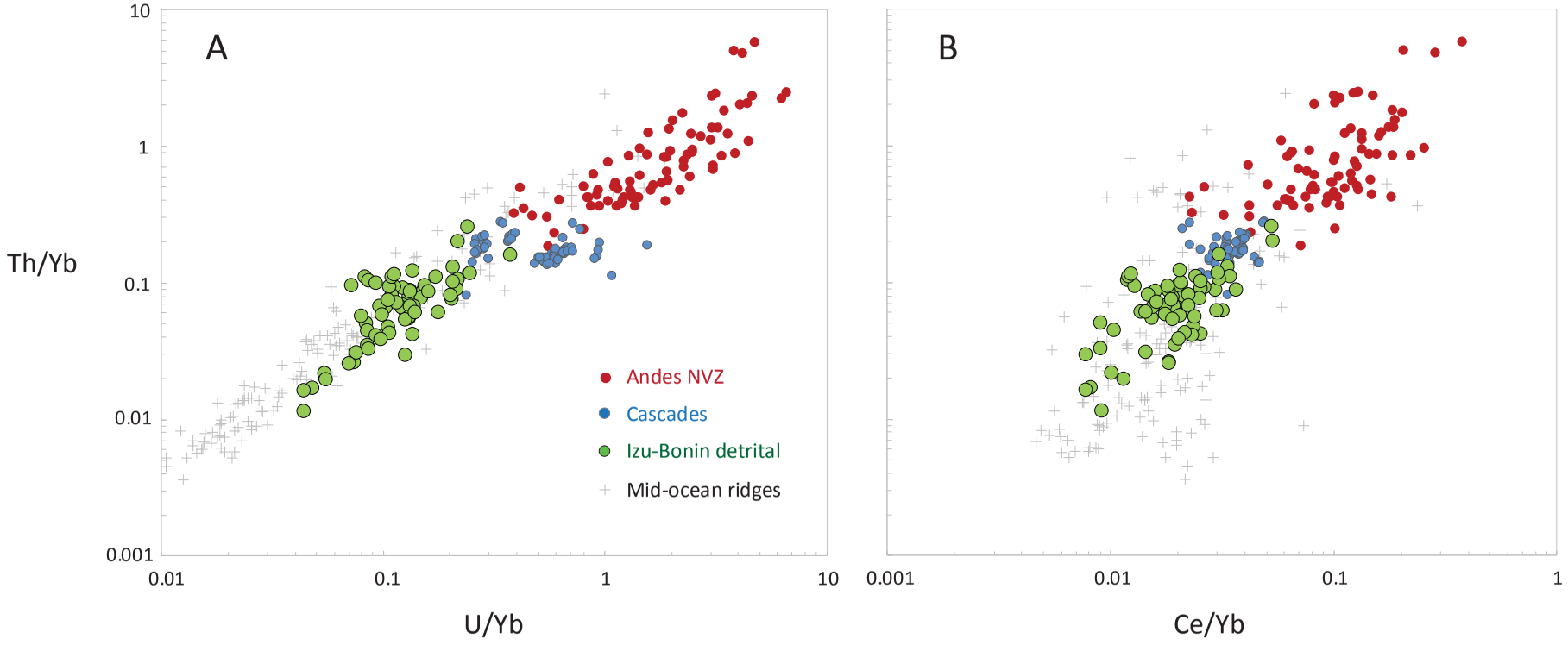

Figure 8.

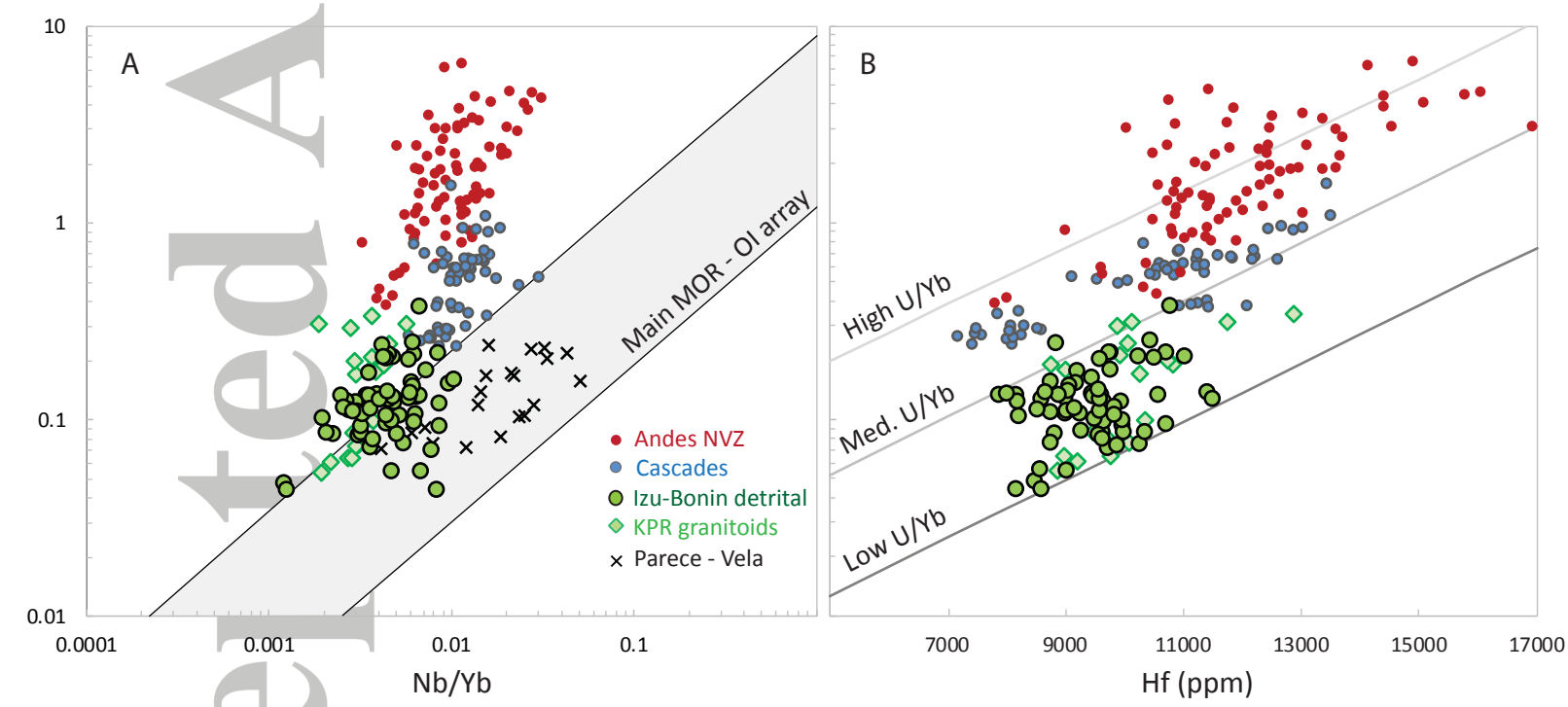

Figure 9.

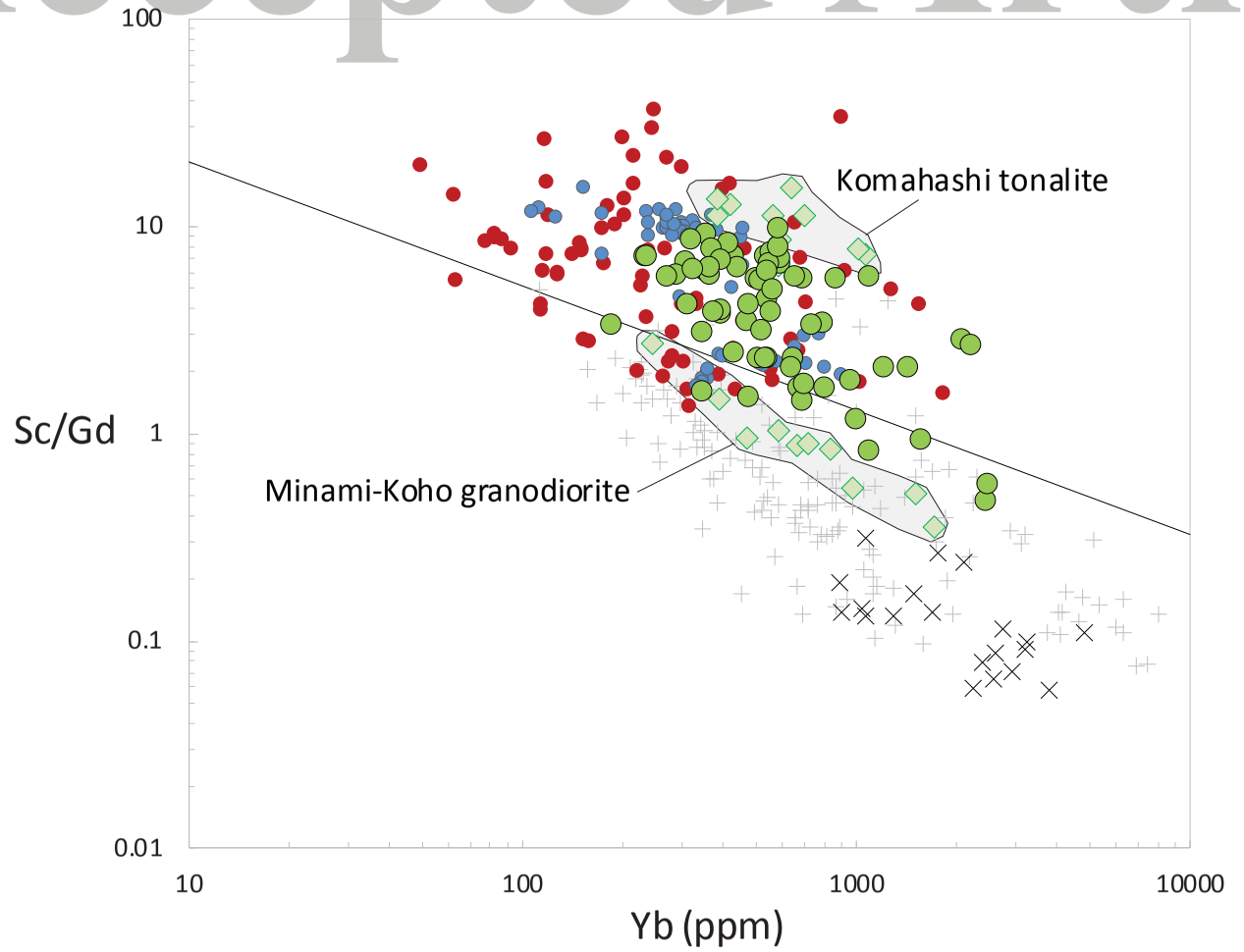

Figure 10.

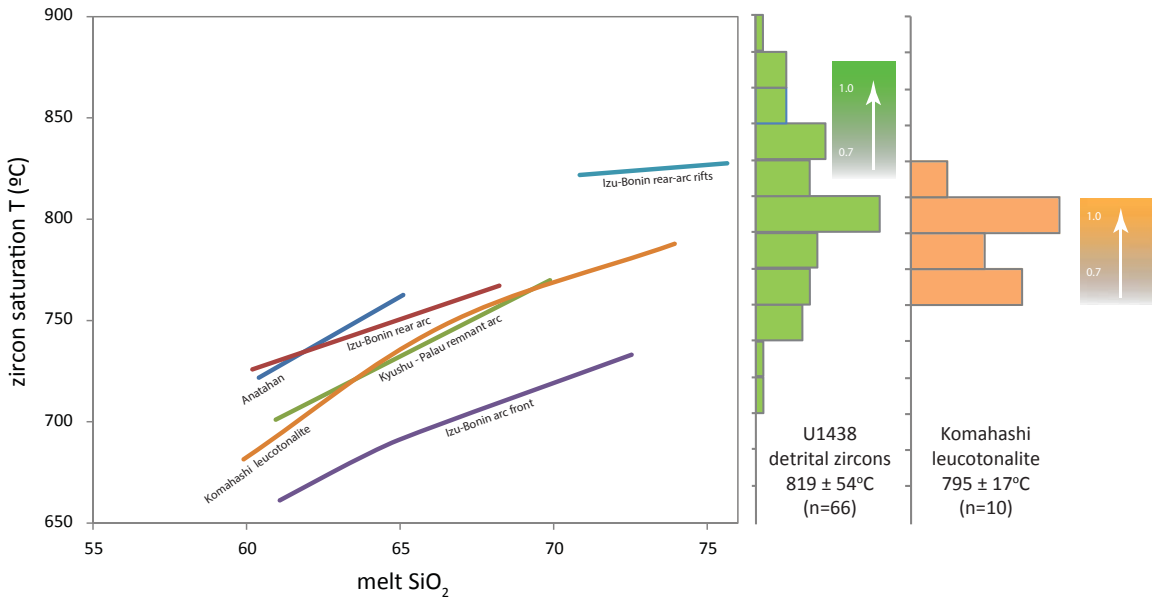

Figure 11.

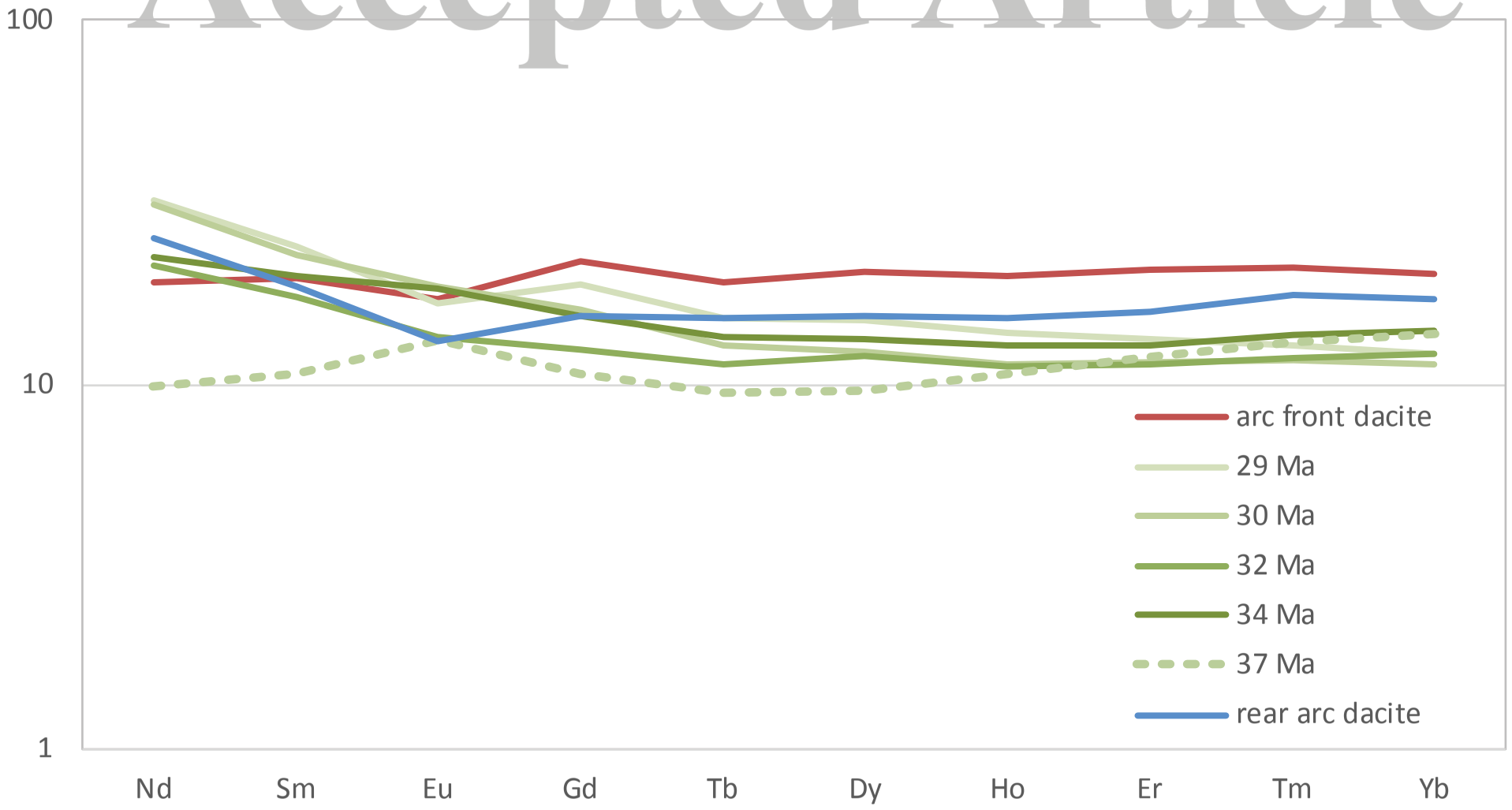

melt/chondrite

Figure 12.